

ECRH Results during Current Ramp-up and Post-Pellet Injection in FTU Plasma

G. Bracco 1), A. Bruschi 1), P. Buratti 1), S. Cirant 2), F. Crisanti 1), B. Esposito 1), D. Frigione 1), E. Giovannozzi 1), G. Giruzzi 4), G. Granucci 2), V. Krivenski 5), C. Sozzi 2), O. Tudisco 1), V. Zanza 1), F. Alladio 1), B. Angelini 1), M.L. Apicella 1), G. Apruzzese 1), E. Barbato 1), L. Bertalot 1), A. Bertocchi 1), G. Buceti 1), A. Cardinali 1), S. Cascino 6), C. Castaldo 1), C. Centioli 1), R. Cesario 1), P. Chuillon 1), S. Ciattaglia 1), V. Cocilovo 1), R. De Angelis 1), M. De Benedetti 1), E. de la Luna 5), F. De Marco 1), B. Francioni 6), L. Gabellieri 1), G. Gatti 1), C. Gormezano 1), F. Gravanti 1), M. Grolli 2), F. Iannone 1), H. Kroegler 2), M. Leigheb 1), G. Maddaluno 1), G. Mafia 1), M. Marinucci 1), G. Mazzitelli 1), P. Micozzi 1), F. Mirizzi 1), S. Nowak 2), F.P. Orsitto 1), D. Pacella 1), L. Panaccione 1), M. Panella 1), F. Papitto 1), V. Pericoli Ridolfini 1), L. Pieroni 1), S. Podda 1), F. Poli 1), G. Pulcella 6), G. Ravera 1), G.B. Righetti 1), F. Romanelli 1), M. Romanelli 1), A. Russo 6), F. Santini 1), Sassi 1), S.E. Segre 3), A. Simonetto 2), P. Smeulders 1), S. Sternini 1), N. Tartoni 1), P.E. Trivisanutto 1), A.A. Tuccillo 1), V. Vitale 1), G. Vlad 1), M. Zerbini 1), F. Zonca 1).

- 1) Associazione Euratom-ENEA sulla Fusione, CR Frascati, CP 65, Frascati, Roma, Italy
- 2) Associazione Euratom-ENEA-CNR, Istituto di Fisica del Plasma, Milano, Italy
- 3) INFN and Dipartimento di Fisica, II Università di Roma "Tor Vergata", Roma, Italy
- 4) Association Euratom-CEA sur la Fusion, DRFC/STPF, CEA/Cadarache, France
- 5) Asociación Euratom/CIEMAT para Fusión, CIEMAT, Madrid, Spain
- 6) ENEA Fellow

e-mail contact of main author: bracco@frascati.enea.it

Abstract. Recent ECRH experiments in FTU have provided new results in two plasma scenarios, both characterized by the absence of the sawtooth activity and by flat or reversed q profiles. The first is the current ramp-up phase where low density plasmas have been heated up to high electron temperature. When the heating is localized on the plasma axis, the high additional power density has produced the evidence of a deformation of the bulk of the local electron distribution function, which is in agreement with the results of a detailed kinetic simulation. When off-axis heating is applied, no clear evidence of non-diffusive energy transport has been found. In the second scenario, ECRH has been applied on the high density plasma produced by pellet injection, resulting in strong ion heating as shown by the increase of the neutron yield. The analysis of this scenario shows that, when the post pellet phase is MHD quiescent, an enhanced energy confinement regime can be obtained with ECRH as found previously in ohmically heated post-pellet plasmas.

1. Introduction

Plasma scenarios where sawtooth activity is absent permit to study the energy transport in the plasma core. In the recent experimental campaigns on FTU ($R=0.93$ m, $a=0.3$ m) ECRH (Electron Cyclotron Resonance Heating) has been applied in two different scenarios, both characterized by the absence of sawtooth activity. In the current ramp-up phase very high values of electron temperature (15 keV) and temperature gradients are achieved with ECRH [1] in low density plasma, in conditions of low electron-ion coupling. Results at higher density have been obtained with pellet injection, where the cooling of the plasma core induced by the pellet inside the inversion radius produces a widening of the current density radial profile that suppresses the sawtooth activity. The post-pellet plasma target is characterized by high electron density, with a peak value near to the cut-off density ($2.4 \times 10^{20} \text{ m}^{-3}$) of the 140 GHz ECRH system [2] and by peaked density profiles. In these conditions clear evidence of ion heating has been obtained. ECRH operates at the fundamental

frequency, with perpendicular, low field side launch and ordinary polarization, so that the resonant magnetic field is 5 T.

The energy transport analysis has been performed using the EVITA code that allows both the interpretative and the predictive time-dependent analysis of a plasma configuration. The code solves the diffusion equations for the poloidal magnetic field, the electron and the ion temperatures using the plasma geometry obtained from the equilibrium reconstruction code, based on the magnetic measurements. Electron temperature is measured by ECE analysis and by Thomson scattering. Plasma density profile is evaluated by the inversion of the line averaged densities measured by a 5 chords DCN interferometer and a 2 chords CO₂ interferometer. In the case of the pellet injection the Thomson scattering density profile are also used in the elaboration. The value of Z effective is obtained by the visible bremsstrahlung signals. Radiation losses are measured by a 12 chords bolometer array. The code evaluates the neutron yield which is compared to the experimental value to obtain information on the ion temperature. Deuterium is the working gas for all the described scenarios. The current density profile is obtained by the solution of the diffusion equation for the magnetic poloidal field and it has been checked that the obtained profiles are consistent with the MHD behaviour of the plasma discharges.

2. Current Ramp-up Experiments

The typical scenario of the current ramp-up experiment is shown in FIG.1. The peak electron temperature attains 14 keV with 0.8 MW on-axis ECRH power at a line averaged plasma density $\langle n_l \rangle = 4 \times 10^{19} \text{ m}^{-3}$. Edge safety factor is $q_a = 5$ at the time of the maximum temperature. Due to the low density the ion temperature is low ($T_i \leq 1 \text{ keV}$). FIG. 2 illustrates the radial profiles of the electron temperature and the radial gradient of the electron temperature exceeds

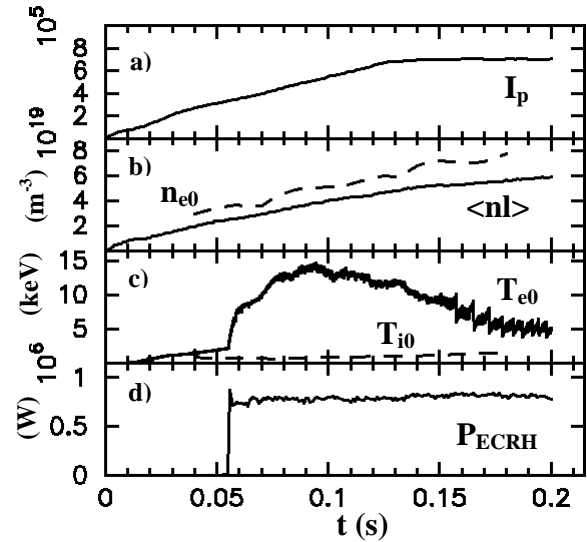


FIG. 1. Time traces for pulse 15020: a) current; b) density (peak and line average); c) temperatures; d) ECRH power (on-axis heating).

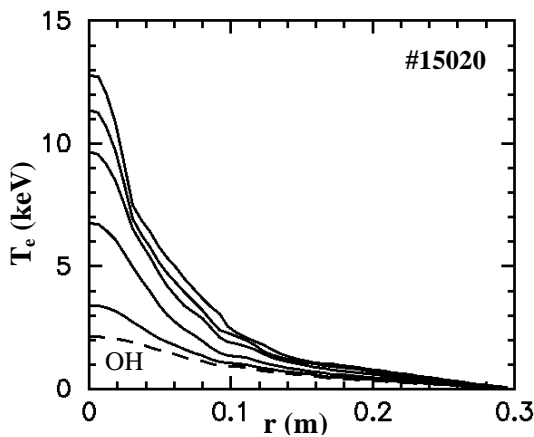


FIG.2 Electron temperature profiles at $t=0.050$ (ohmic,dashed), 0.060, 0.070, 0.080, 0.095 s for on-axis ECRH.

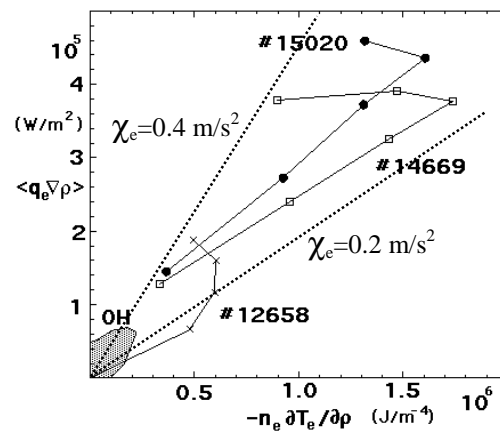


FIG.3. Energy flux versus nVT in the core ($r/a < 0.15$) at the time of maximum temperature for on-axis ECRH (12658 0.4 MW, 14669 and 15020 0.8 MW)

200 keV/m. The global energy confinement of these discharge is close to L-mode scaling values (ITER89-P) and ohmic power is of the same order as the additional power. In the plasma core however the ECRH power is largely the dominant term so that the local energy transport analysis can be performed in detail. The results of the interpretative analysis are shown in FIG. 3 for the same plasma discharge where the local energy flux is plotted versus $n_e \nabla T_e$ so that a given value of the electron thermal diffusivity χ_e corresponds to a fixed slope in the plot. Experimental data for the plasma core lie in range $\chi_e = 0.2 \div 0.4 \text{ m}^2/\text{s}$ as the ohmic data, but at a much higher value of electron temperature and electron temperature gradient. Previous data at a lower ECRH power (0.4 MW) are also shown, with no evidence of degradation of energy confinement in the plasma core with increasing power.

2.1 The effect of different current profiles

In the current ramp-up phase the plasma target is characterized by a variety of shapes of the current profile, that depends on the plasma start-up characteristics, gas filling, impurity content. As a consequence it has been possible to inject ECRH in plasma both with hollow and peaked current profiles to study the consequences induced to the electron energy transport. The data illustrated in FIG.1-3 correspond to a case where pre-ECRH temperature and current profile is peaked. The MHD behaviour of the discharge is characterized by a low activity until the sawtooth starts, FIG.1. FIG. 4 shows the case of a very hollow pre-ECRH temperature profile: peak T_e reaches 15 keV with 0.9 MW on-axis ECRH, but a strong

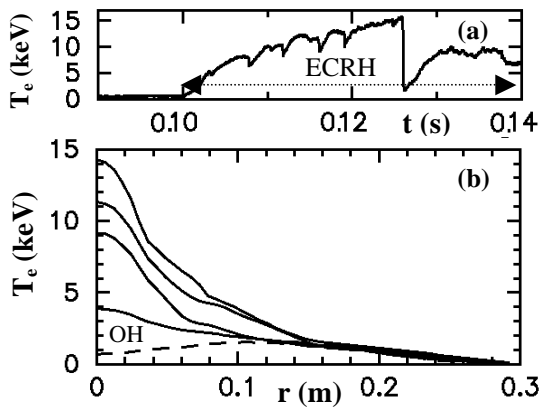


FIG.4. pulse 17389, (a) peak T_e versus time; (b) T_e radial profiles at $t=0.098$ (ohmic-dashed), 0.108, 0.113, 0.118, 0.123 s, with 0.9 MW on-axis ECRH.

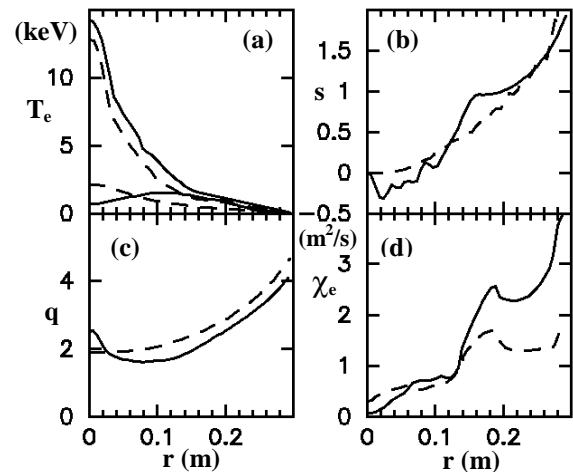


FIG.5. Comparison between pulse 15020 (dashed) and 17389 (full) at the time of maximum temperature; (a) $T_e(r)$, ohmic data also shown; (b) $q(r)$; (c) magnetic shear $s(r)$; (d) $\chi_e(r)$.

reconnection quenches the electron temperature increase when the minimum value of safety factor q becomes lower than 2. FIG. 5 compares the two cases with different current profiles: the values of the electron thermal diffusivity in the plasma core seems similar but it must be noticed that q profiles are characterized by a low magnetic shear in then plasma core ($s \leq 0.5$) for both cases.

2.2 Off-axis heating experiments

Off-axis heating experiment have been performed, either by changing the location of the resonance layer by changing the value of the toroidal magnetic field B_t or by tilting ECRH launchers. In the latter case the power deposition is broader. In FIG. 6 the results of a radial

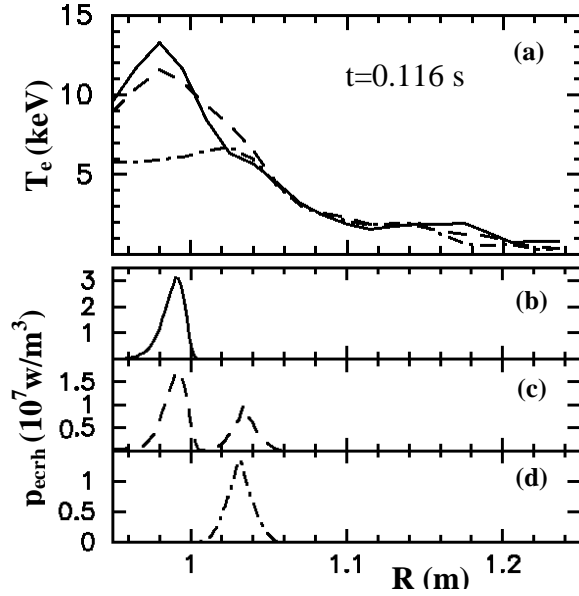


FIG. 6. Radial scan of power deposition, pulses 17389 (full), 17392 (dash), 17393 (dash-dot); (a) T_e profiles, (b,c,d) ECRH power density.

scan of power deposition at fixed B_t value are shown. In three different pulses the two launchers were set respectively both at the plasma center, one at center one off-axis, both off-axis. The shape of the electron temperature profile follows what is qualitatively expected from a diffusive model for the plasma energy transport. The interpretative transport analysis is rather critical for off-axis experiments due to the uncertainty in the power deposition profile so a predictive approach has been applied. The pulses were characterized by hollow pre-ECRH temperature and current profiles. On-axis experiment were previously [3] successfully simulated by using the Bohm term of the mixed shear Bohm Gyro-Bohm model [4] for on-axis heating on peaked pre-ECRH profiles. The same approach is not successful in the case of hollow current profiles as the model sets $\chi_e \approx 0.0$ for magnetic shear $s \leq 0$ resulting in extremely hollow electron temperature profiles. To show the compatibility of the results with a diffusive model, the data of the full off-axis case have been simulated, FIG. 7, using an ad-hoc electron thermal diffusivity profile, constant in time, with a value in the range 0.2-0.5 m^2/s in the plasma core. FIG. 8 shows the result of an off-axis heating experiment where the localization of the resonance has been changed by changing B_t value, in the case where the pre-ECRH profiles are peaked. In this case the data can be reproduced by using the functional form of the Bohm term of the mixed shear Bohm Gyro-Bohm model, multiplied by a factor 2.

2.3) High electron temperature on current flat top

When the start-up phase produces a plasma with hollow electron temperature and current density profiles there are cases where this feature persists also in the current flat-top

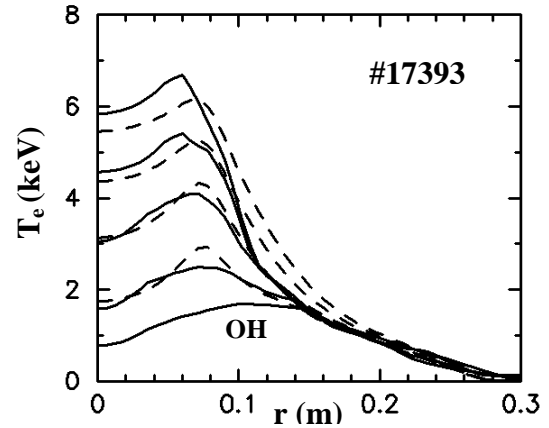


FIG. 7. Electron temperature profiles at $t=0.098$ (OH), 0.103, 0.108, 0.113, 0.118 s for off-axis 0.9 MW ECRH; full line experimental, dashed simulation.

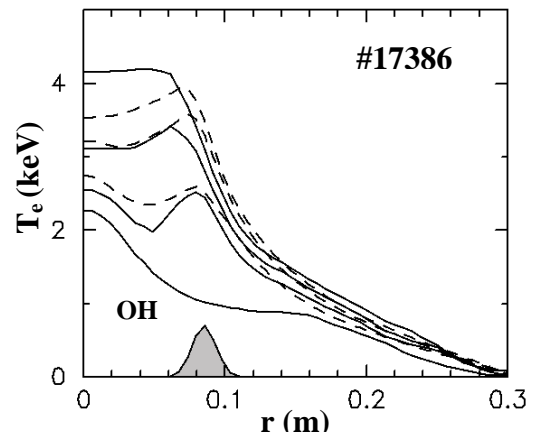


FIG. 8. Electron temperature profiles at $t=0.096$ (OH), 0.106, 0.11, 0.116 s for off-axis 0.9 MW ECRH; full line experimental, dashed simulation; the shaded area indicates the power deposition localization.

phase. This is due to high radiation from the plasma core, so that the local ohmic power is balanced by radiation losses at the plasma center. On axis ECRH heating has been applied to such a plasma, FIG. 9, and a peak T_e value in excess of 10 keV has been obtained at the same density characterizing the current flat-top scenario ($\langle n \rangle = 4 \times 10^{19} \text{ m}^{-3}$), at a plasma current $I_p = 0.4 \text{ MA}$. The local analysis of the ohmic phase of this pulse shows that indeed the balance between ohmic power and radiation losses in the center while the q profile appears to be hollow with $q_0 \approx 3$ and $q_{\min} \approx 2$. The plasma is MHD quiescent until the development of the saw-tooth activity. The T_e profile at the time of the maximum temperature is narrower than in the ramp-up cases FIG.2, 4, possibly due to the reduced width of the low shear ($s \leq 0.5$) region. The value of Z effective is $Z_{\text{eff}} = 3$ in this scenario, while current ramp-up phase has much higher values $Z_{\text{eff}} = 7 \div 10$. The pulse demonstrates that high T_e values can also be obtained on the current flat-top phase, provided that the current profile is far from the standard sawtooth regime. In this pulse comparison between the experimental neutron yield and the estimate using a the ion temperature evaluated using Chang-Hinton ion thermal diffusivity, shows a degradation of the ion transport during the high electron temperature phase. Indication of density pump-out are also observed.

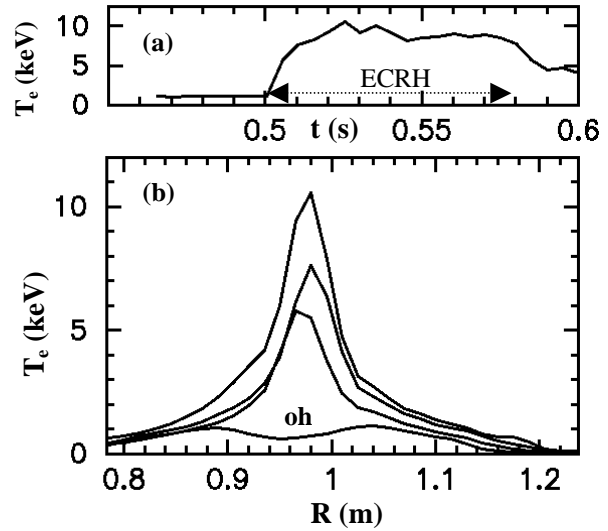


FIG. 9. pulse 17578, (a) peak T_e versus time; (b) T_e radial profiles at $t = 0.486$ (OH), 0.506, 0.511 and 0.525 s, with 0.9 MW on-axis ECRH on current flat

2.4) Electron Temperature Measurements

The present set-up of the Thomson Scattering diagnostics on FTU is not well suited for high electron temperature plasma ($T_e > 10 \text{ keV}$) due to the chosen spectral range. Therefore the measurement must rely on ECE analysis. The full ECE spectra including 2nd, 3rd and 4th harmonics is shown in FIG. 10 for a high electron temperature plasma pulse. A hump at the low field side (i.e. low frequencies) is observed in the experimental data, due to the relativistic down shifted emission from the central electrons, not reabsorbed by plasma periphery. A simulation of the spectra using the measured peak electron temperature $T_{e0} = 15 \text{ keV}$ shows that the intensity of this hump should be much greater than observed, as also the other features at the 3rd and 4th harmonics. The full spectra except the 2nd harmonic peak can be

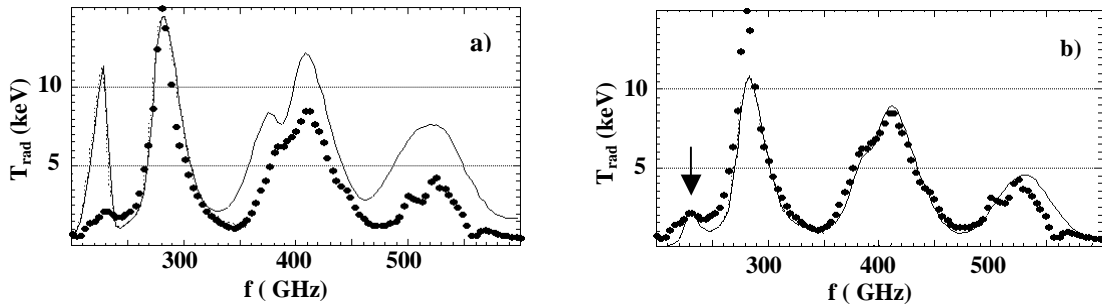


FIG. 10 ECE spectra for a high T_e discharge, experimental data (dots) are compared with simulations assuming a) $T_{e0} = 13.5 \text{ keV}$ and b) $T_{e0} = 11.5 \text{ keV}$; low energy deformation of the electron distribution function is not included. 2nd harmonics is located at 280 GHz. The arrows indicate the low frequency hump.

reproduced by a lower $T_{e0}=11$ keV. The discrepancy can be solved by taking into account the distortion of the low energy distribution function due to the high ECRH power density in conditions of low collisionality: high temperature and low plasma density [5,6]. A high poloidal resolution Fokker-Plank code has been run for plasma parameters typical of the high electron temperature plasma pulses. The deformed distribution function is isotropic and the deviation from a Maxwellian is concentrated in the range 10–20 keV. The consequences of the deformation of the electron distribution function on the ECE spectra are shown in FIG.11 where the ratio between the peak and the hump intensity is in good agreement with the data shown in FIG. 10. The effect is important only in the ECRH deposition layer, near to the magnetic axis while the measurement of the electron temperature in the gradient region is unaffected. Also the Thomson Scattering measurement is sensitive to the deformation of the electron distribution function but the effect is quantitatively smaller. Another result from the code is that the energy content of the deformed low energy distribution function is near to the value corresponding to the nominal temperature value, so that even the estimate of core energy appears to be correct.

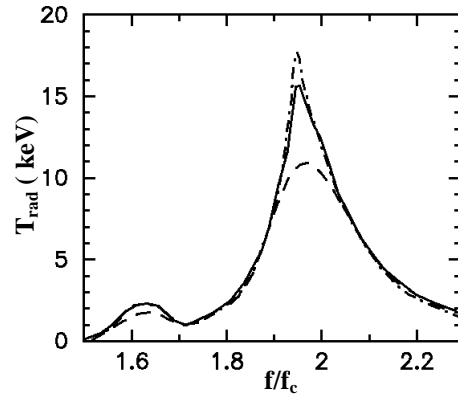


FIG.11 ECE radiation temperature versus normalized frequency: Maxwellian distribution function (dashed); with distribution function deformation for on axis (dot dashed) and 1 cm off-axis (full) deposition,

3) Pellet Experiments

Ohmic plasma in the post-pellet phase are characterized in FTU by the suppression of the sawtooth activity, by peaked density profiles, by the reduction of the ion energy transport to the neoclassical value and by an improved global energy confinement [3]. ECRH has been applied in this scenario to check if these features are maintained with additional electron heating. The cut-off density at 140 GHz ($2.4 \times 10^{20} \text{ m}^{-3}$) sets a strong constraint to the experiment, as the pellet injector system was designed to inject deuterium pellets of a size ($1-2 \times 10^{20}$ atoms) permitting to explore the high density limit of a high field tokamak. To fulfil the constraint a low density plasma target ($\langle n_l \rangle \leq 1 \times 10^{20} \text{ m}^{-3}$) has been chosen and off-axis ECRH has been applied. The results obtained for a plasma pulse at $I_p=0.6$ MA, $B_T=5.6$ T, ($q_a=4.8$) are shown in FIG.12. ECRH power (0.8 MW) is applied 50 ms after

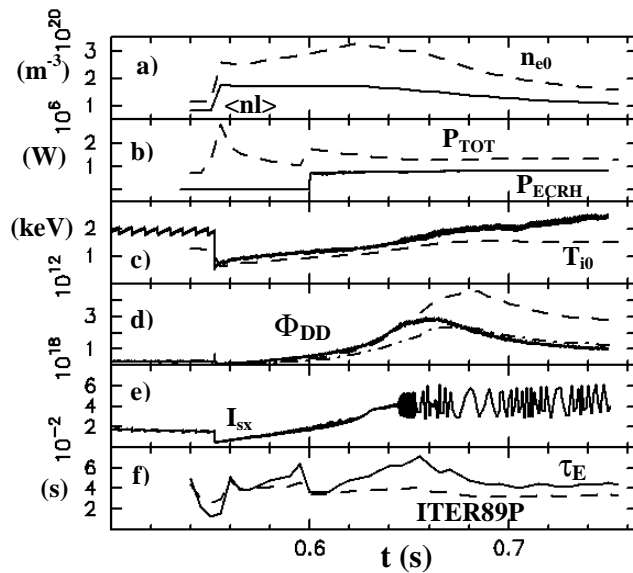


FIG. 12. Time traces for pulse 17839, pellet injected at $t=0.55$ s: a) peak and line averaged density; b) total and ECRH power; c) peak electron and ion temperature; d) neutron yield: experimental (full), neoclassical (dashed), 2 times neoclassical (dot-dashed); e) soft X emission; f) global energy confinement time: experimental (full), ITER89-P (dashed).

the pellet, in a phase when the line averaged density is very slowly decreasing, while peak density is slightly increasing so that density profiles are peaking. MHD activity is rather quiescent as the sawtooth is suppressed by the pellet. The plasma reheating is helped by ECRH, electron temperature and neutron yield increase up to the time when a strong central $m=1$ mode starts. At that point the neutron yield increase is quenched, density decreases and density peaking is reduced. The global energy confinement time that has reached transiently 1.5 times the value of the ITER89-P scaling returns near to the L-mode value. The comparison between the experimental neutron yield and the estimate produced by the solution of the ion energy diffusion equation using Chang-Hinton ion thermal diffusivity shows that before the $m=1$ mode the neoclassical value is in agreement with the experiment, while during the mode the ion diffusivity increases of a factor 2. In FIG.13 the electron density and temperature profiles are shown together with the radial location of the ECRH power, for times before the $m=1$ mode onset. The additional power is deposited just below the cut-off layer at $2.4 \times 10^{20} \text{ m}^{-3}$ and symptoms of density pump-out in the deposition region are observed. The evolution of the temperature profiles shows the characteristics of a diffusive behaviour, similarly as in the low density high temperature case of section 2.

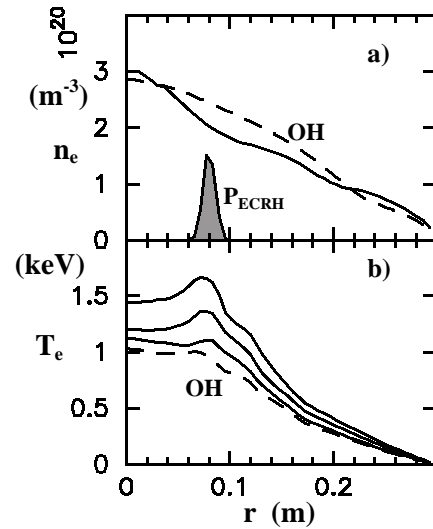


FIG.13. Pulse 17389, radial profiles: a) electron density, at $t=0.595$ s (OH-dashed), $t=0.650$ s (ECRH-full), shaded area marks the power localization; b) electron temperature at $t=0.595$ s (OH-dashed), $t=0.610, 0.630, 0.650$ s (full).

The current profile as evaluated from the diffusion equation for the poloidal magnetic field is very flat in the core region, including the deposition layer, as magnetic shear $s \leq 0.5$ for $r/a \leq 0.5$. The same scenario has been performed also at higher plasma current, 0.76 MA, $q_a=3.7$ with qualitatively similar results as far as the time behaviour of the main quantities is concerned. Quantitatively the lower q_a case shows only a marginal confinement improvement over the L-mode and no clear reduction of ion energy transport can be deduced from the experiment. The neutron yield increases of about 20 % up to 3.5×10^{12} n/s essentially due to the broader temperature profiles.

Some experiments have been performed in a similar scenario displacing the resonance layer to the plasma center. The on-axis heating induces a fast onset of the sawtooth activity and a stronger density pump-out has been observed.

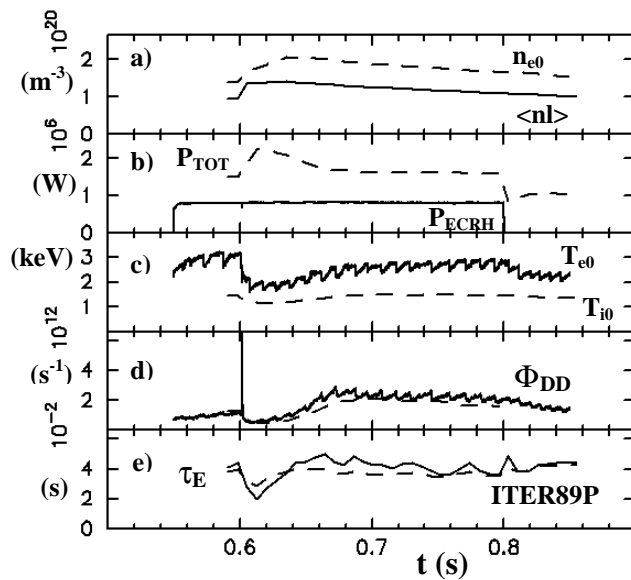


FIG. 14. Time traces for pulse 17844, pellet injected at $t=0.6$ s: a) peak and line averaged density; b) total and ECRH power; c) peak electron and ion temperature; d) neutron yield: experimental (full), computed with χ_i 5 times Chang-Hinton (dashed); e) global energy confinement time: experimental (full), ITER89-P scaling (dashed).

To reduce the density increase produced by the pellet the scenario where the pellet injection is performed on a plasma heated by off-axis ECRH has also been performed. In that case the higher electron temperature induces a more peripheral deposition of the pellet particles. The results are shown in FIG.14 where density, power, temperature, neutron yield and global confinement time are plotted versus time for a pulse at 0.76 MA, $q_a=3.7$. In this case the pellet injection is not able to suppress sawtooth activity that persists. In this last plasma scenario the improvement on the global energy confinement and on the ion energy transport are not observed.

4. Conclusions

The experiments with ECRH in the current ramp-up scenario show that low values of electron thermal conductivity, comparable to the values measured in the core of ohmic plasma discharges, are observed in the plasma core at a much higher values of electron temperature and electron temperature gradients. The comparison between plasmas with different shapes of current density profiles indicates that the low thermal conductivity region could be correlated with a low or negative value of the magnetic shear. It has also been shown that similar results can also be obtained in the current flat-top phase in cases when the current profile is far from the standard sawtooth scenario. The experiments where ECRH has been injected in the post-pellet phase show that the improvement in the energy confinement and in the ion energy transport, probably correlated with peaked density profiles, can be obtained also with additional electron heating. An interesting feature of both scenarios is that the electron temperature profile in the core region does not show indication of profile resiliency and can be interpreted as the result of a diffusive transport mechanism far from a critical gradient regime. This observation is found for ECRH in the plasma core both in the low density, high temperature case of the current ramp-up experiments and in the high density, low temperature case of the post-pellet plasma phase. Other experiments with more peripheral ECRH on low current discharges have produced qualitatively different results in FTU [7] where indication of profile resiliency are clearly found. The different behaviour could be correlated with the different magnetic shear values in the deposition region of the additional power between the two different experimental scenarios or to the proximity to a critical gradient regime in the experiments of ref. [7].

- [1] P. Buratti, et al., "High core electron confinement regimes in FTU plasma with low or reversed magnetic shear and high power density electron-cyclotron-resonance heating", Phys. Rev. Letters 82 (1999) 560.
- [2] S. Cirant et al. "Long pulse ECRH experiments at 140 GHz on FTU tokamak", Proc. of 10th Joint Work. on ECE Emiss. and ECRH, T. Donne' and Toon Verhoeven Editor, 369 (1997).
- [3] G. Bracco et al. "Energy transport analysis of high temperature and high density FTU plasma discharges", 17th IAEA Fusion Energy Conf., 1998, Yokohama, EXP2(01).
- [4] Vlad G., et al., "A general empirically based microinstability transport model", Nucl. Fusion 38 (1998) 557.
- [5] O. Tudisco et al. " Electron Cyclotron Heating experiments during the current ramp-up in FTU " 26th EPS, Maastricht 1999.
- [6] V. Krivenski.-"High-Resolution Kinetic Simulations of Electron Cyclotron Heating"- 13th Topical Conf. Applications of RF power to Plasmas - Apr. 12-14, 1999 - Annapolis.
- [7] C. Sozzi et al. "Energy confinement and Sawtooth Stabilization by ECRH at High Electron density in FTU tokamak", this conference, paper EXP5/13.